Toxicology Research

Accepted Manuscript

ROYAL SOCIETY OF CHEMISTRY

www.rsc.org/toxicology

Title

Impact of manganese on the hippocampus metabolism in the context of MEMRI: a Proton HRMAS MRS study

Short title

Impact of manganese on the hippocampus metabolism

Authors

A. Daoust[1,2], E. L. Barbier[1,2], S. Bohic[1,3], V. Stupar[1,2], S. Maunoir-Regimbal[4] and F. Fauvelle[4]

[1]Inserm, U836, Grenoble, France
[2]Université Grenoble Alpes, Grenoble Institut des Neurosciences, Grenoble, France
[3]European Synchrotron Radiation Facility (ESRF), Grenoble, France
[4] IRBA-CRSSA, Grenoble, France.

Alexia DAOUST, daoustalexia@hotmail.fr
Emmanuel Barbier, emmanuel.barbier@ujf-grenoble.fr
Sylvain BOHIC, bohic@esrf.fr
Vasile STUPAR, vasile.stupar@ujf-grenoble.fr
Séverine MAUNOIR-REGIMBAL, severine.maunoir-regimbal@irba.fr
Florence FAUVELLE, florence.fauvelle@ujf-grenoble.fr

Corresponding author

Dr Emmanuel Luc BARBIER, PhD
Inserm unite 836
Chemin Fortuné Ferrini
BP 217 – CHU Grenoble
F-38043 Grenoble cedex, France
Tel: +33 4 56 52 05 88
Fax: +33 4 56 52 05 98
E-Mail: emmanuel.barbier@ujf-grenoble.fr

Abstract words count:
Text words count (text without abstract, acknowledgments, references, tables, and legends): 4420
Tables: 0
Figures: 6
Supplemental information: 2

Key-words

HRMAS, proton, spectroscopy, Manganese, MEMRI, metabolism, rat, brain

Abbreviations

Ace: acetate
Ala: alanine
Asp: aspartate
Cr: creatine and phosphocreatine
Cho: choline
DH: Dorsal hippocampus

GABA: γ-amino-butyric acid
Glu: glutamate
Gln: glutamine
Gsh: glutathione
GPC: glycerophosphocholine
Gly: glycine
HRMAS: High resolution magic angle spinning
IH: intermediate hippocampus
Lac: lactate
MEMRI: Manganese enhanced magnetic imaging
m-Ins: myo-inositol
NAA: N-acetylaspartate
PE: phosphoethanolamine
PC: phosphocholine
S-ins: scyllo-inositol
Tau: taurine
VH: ventral hippocampus

ABSTRACT

Manganese enhanced MRI (MEMRI) offers many possibilities such as tract tracing of neuronal pathways and functional imaging *in vivo*. This technique necessitates a direct or indirect acute injection of $MnCl_2$ in the brain. Unfortunately, local concentrations of Mn^{2+} and its impact on metabolism after a single injection remain largely unknown. In this study, we combined *in vivo* MEMRI and *ex vivo* Proton High Resolution Magic Angle Spinning MRS (^{1}H HRMAS MRS) to investigate the delayed impact of Mn^{2+} on rat hippocampal metabolism MEMRI images were acquired 24h after $MnCl_2$ injection in the dentate gyrus of the rat hippocampus at two different Mn^{2+} doses: low (8 nmol; n=16) and high (500 nmol; n=10). The low Mn^{2+} dose had almost no impact on hippocampal metabolism while the high dose altered the amplitude of several metabolites (up to +54% for Glu and -71% for Asp). Moreover, at this high dose, the paramagnetic properties of Mn2+ lead to broadening of resonances of several organic acids (lactate, glutamate, N-acetyl aspartate…), suggesting a chelation of Mn^{2+} and an impact on Mn^{2+} relaxivity. Metabolite amplitudes were well correlated with the Mn^{2+} concentration measured with MRI T_1-map (glutamate: R^2= 0.8, p=0.02; phosphoethanolamine: R^2=0.9, p=0.0004; γ-aminobutyrate: R^2= 0.7, p=0.005 and phosphocholine: = 0.6, p=0.04). To conclude, HRMAS is well suited to investigate Mn^{2+} impact on metabolism. The low Mn^{2+} dose (8 nmol) usually used in MEMRI experiment does not impact the hippocampal metabolism. The chelation of Mn^{2+} and its impact on relaxivity suggests an over-estimation of Mn^{2+} concentration when measured through T_1 map.

INTRODUCTION

Manganese (Mn^{2+}) is an essential metal for brain functions [1]. It is a cofactor of several enzymes involved in neurotransmitter synthesis and is essential to process amino acid, lipids, proteins and metabolites such as dopamine and serotonin [2]. Manganese enhanced MRI (MEMRI) technique [3] relies upon the paramagnetic properties of Mn^{2+}. Further, Mn^{2+} is able to enter neurons through voltage dependent Ca^{2+} channels [4] and can then be actively transported along axons and can cross synapses [5]. These properties make Mn^{2+} a unique contrast agent for enhancing brain cytoarchitecture, functional studies and tracing neuronal connections [3]. This last application, also called tract-tracing, is more and more used in research [6–8]. It necessitates an acute injection of Mn^{2+} at the starting point of the studied tract, for example the brain [6,9], the eye [8] the nostril [10] or the ear [7]. All of these studied tracts have a direct or indirect input in the brain, meaning that Mn^{2+} is transported along the tract inside the brain. While several studies have shown that chronic intake of Mn modifies brain metabolism [11–14], few is known about Mn^{2+} impact on brain function and Mn^{2+} local concentrations after an acute injection. It is however known that at a cellular level, a high dose of Mn^{2+} induces mitochondrial dysfunction and disrupts the cellular energy metabolism [12,15–17]. All these data highlight the need of further experiments to validate Mn acute injection for MEMRI purpose. The aim of this work was to evaluate the impact of an acute intracerebral injection of Mn^{2+} on the hippocampus metabolism, a structure chosen for its ability to accumulate Mn^{2+} [18] and for its interest in previous MEMRI studies focused on Alzheimer disease[19].

A high (500 nmol) and a low (8 nmol) dose of $MnCl_2$ were used in this study. The high dose was chosen from previous MEMRI studies which used between 160 and

800 nmol of $MnCl_2$ [20,21] and is in line with our previous study [22]. This high dose is a positive control for Mn^{2+} disturbance of hippocampus metabolism.

The low dose was selected from different applications of tract tracing in which authors used between 1.25 and 16 nmol of $MnCl_2$ [9,20,23]. Tissular metabolism was characterized using *ex vivo* Proton High Resolution Magic Angle Spinning MRS (^{1}H HRMAS MRS). This method, like *in vitro* liquid high resolution NMR, allows the characterization of the metabolic phenotypes of cells, tissues and organs, with high sensitivity and resolution (compared to *in vivo* MRS). Indeed, about twenty metabolites can be detected and quantified by using this technic [24]. Moreover, HRMAS MRS has the additional advantage of avoiding extraction or chemical treatment [25], so small intact biopsies can be analyzed (10 to 15 mg). This latter allowed us to investigate the concentration gradient of Mn^{2+} along each ipsi- and contralateral side of hippocampus, by dividing them in three equal parts: dorsal, intermediate and ventral hippocampus

RESULTS AND DISCUSSION

MEMRI

As expected, for all animals who received the high dose of Mn^{2+} (500 nmol), a hyperintense T_1-weighted signal was observed 24 h after Mn^{2+} injection (**Fig. 1A**), more pronounced in the DG and CA3 of the hippocampus. The signal in both the ipsi- and the contralateral hippocampus was enhanced, in line with our previous results [22]. After the low dose of Mn^{2+} (8 nmol), signal hyperintensities were only visible in the ipsilateral DG and in the CA3 of the hippocampus (**Fig. 1A**).

Estimation of Mn^{2+} concentration in hippocampus by MRI

Mn^{2+} concentration was derived from T_1 values measured in each ROI (**Fig.1 Supp**). Twenty-four hours after Mn^{2+} injection, there was a decreasing gradient of Mn^{2+} concentration along the hippocampus from the ipsilateral dorsal hippocampus (DHi, injection site) to the ipsilateral ventral hippocampus (VHi, **Fig. 1B**). Mn^{2+} concentration are resumed in Fig. 1C. For the low Mn^{2+} dose (8 nmol), Mn^{2+} concentrations varied from 93 to 35 µM in hippocampi and were significantly higher than that of control only in DHi, IHi and DHc. For the high Mn^{2+} dose (500 nmol), Mn^{2+} concentrations varied from 870 to 115 µM and were significantly higher than that of control in the entire hippocampus, for both ipsi- and contralateral sides. No difference was observed between controls who received the vehicle injection corresponding to low and high doses.

INSERT FIG. 1

Paramagnetic effect of Mn^{2+} on *^{1}H HRMAS MRS* spectra

HRMAS spectroscopy was performed on 3 biopsies of each ipsi- and contralateral hemisphere. The average weight of the biopsy was 15±0.5 mg with no difference between biopsies originated from control and Mn^{2+} injected animals (p=0.9).

For control rats (vehicle injection), a highly resolved spectrum was obtained by ^{1}H HRMAS MRS in the 0.5-4.5 ppm spectral region, with sharp resonances for all metabolites (3 Hz) (**Fig. 2)**. The same feature was observed for low Mn^{2+} dose. Conversely, after injection of the high Mn^{2+} dose (500 nmol), the spectra were strongly perturbed at the injection site (DHi): Lac, NAA, Glu and Asp resonances were broadened (**Fig. 2**, arrows), whereas other resonances remained nearly as sharp as in the control spectrum. Among NAA resonances, the aspartyl part of the molecule was more broadened than the acetyl part. The methyl group of Lac gave rise to one of the highest peaks of the biopsy spectra, allowing reliable measures of its linewidth, unlike the methyl group at 4.12 ppm or aspartate resonances (**Fig. 2**), which were nearly unresolved in DHi biopsy after Mn^{2+}. The mean linewidth of lactate was 10.5 Hz in DHi, 9.9 Hz in IHi, 9.6 Hz in DHc and 9.3 Hz in IHc. We observed a decrease in line broadening along the right hippocampus, whereas no broadening was observed in the left hippocampus. These results suggest that Lac broadening, as well as that of Asp, Glu and NAA, could result from a specific chelation of Mn^{2+}. To test this hypothesis, *in vitro* competition experiments were performed.

INSERT FIG. 2

In vitro ^{1}H HRMAS MRS of Mn^{2+} solutions

Resonance broadening of Lac and m-Ins

Since we did not detect any broadening for m-Ins in our biopsy spectra (**Fig. 2**), it was selected for a competition experiment with Lac for Mn^{2+} chelation. **Fig. 3** shows the plot of Lac and m-Ins linewidth versus the Mn^{2+} concentrations, measured in *in vitro* spectra of a solution containing 8 mM of Lac and 8 mM of m-Ins in the presence of varying amounts of Mn^{2+}. The m-Ins linewidth does not vary in the presence of Mn^{2+}, whereas Lac broadening is strongly correlated to the Mn^{2+} concentration.

These effects were only observable when Mn^{2+} amounts remained sufficiently small to avoid a global paramagnetic effect, e.g. for a Mn^{2+} concentration lower than 125 µM in this experiment. The same experiment was then repeated without m-Ins and produced a similar result with a regression line slope of 0.0673 and correlation coefficient of R^2=0.97 (data not shown). These results clearly indicate that a specific chelation could occur between Lac and Mn^{2+}.

INSERT FIG. 3

T_1 in the presence of high Mn^{2+} dose

The T_1 of water protons, whether pure or with Lac (8 mM) was about 5.5 s. In presence of Mn^{2+} (20 µM), the T_1 of water protons was more reduced in the 8 mM Lac solution (T_1=2.9 s) than in pure water (T_1=3.4 s). Moreover, the T_1 of the Lac CH group was more reduced after Mn^{2+} addition (-92%) than that of the CH_3 Lac group (-65%).

Mn^{2+} impact on hippocampal metabolism

For the high Mn^{2+} dose, the quantification was achieved by using a metabolite database with specific broad resonances. Using this approach, it was possible to properly quantify the corresponding metabolites (Lac, NAA, glu and Asp), since CRLB were of the same order of magnitude than without broadening (see Methods section). Moreover, a good data homogeneity was obtained in the vehicle-injected group (5%<SD<10% for most of the metabolites) allowing detection of metabolic variations after Mn^{2+} treatment.

High dose Mn^{2+} injection (500 nmol*)*

In the ipsi and contralateral hippocampus, strong metabolic variations were measured after Mn^{2+} injection. The injection site (DHi) and its contralateral equivalent (DHc) were the most affected hippocampal parts. Metabolic variations decreased

along the hippocampus. At the injection site (DHi), 8 metabolites were significantly modified: Ala and Glu increased, respectively, by 34% and 54% relative to control DHi, whereas Asp (-71%), GABA (-17%), PC (-14%), PE (-37%), Lac (-10%) and NAA (-19%) were significantly decreased (**Fig. 4**). In the IHi, metabolite levels were less impacted by Mn^{2+}: Ala and Asp did not differ from that of the control hippocampus, whereas m-Ins decreased (-16%). The other metabolites GABA (-25%), PC (-16%), PE (-53%), Lac (-13%) and NAA (-12%) remained significantly lower than in control tissue. Finally, in VHi, all metabolites were comparable to that of control tissue; in addition, Ala (12%) and NAA (-6%) remained slightly different than in control tissue (data not shown). In the contralateral hippocampus, metabolic perturbations were also important mainly in the DHc, with 7 metabolites that varied significantly. Interestingly, the same metabolic variations were observed in DHc and in DHi, except for Asp and GABA: Ala and Glu significantly increased by 11 and 56%, respectively, whereas PC, PE, and NAA decreased by -15, -36, and -13%, respectively. Moreover, m-Ins (-16%) and Cho (-15%) also decreased. In IHc and VHc, only PE was significantly reduced (-22% and -15%, respectively). Ace, Gln, GSH, GPC, Gly, Pcr and Tau were not significantly modified in any of the structures. **Figure 5** shows the relative change in metabolite (Glu, GABA, PC and PE) amplitude with respect to their control value. We clearly see that the metabolite perturbation decreases along the hippocampus for both the ipsi- and contralateral hippocampus. All metabolites were normal in the VH, except Ala (12%) in ipsi- side, PE (-15%) in contra-side and NAA in both ipsi- (-6%) and contra- (-5%) sides.

*Low dose Mn^{2+} injection (*8 nmol*)*

The impact of Mn^{2+} on metabolism was much less important than for the high dose (see above). We observed a significant decrease of NAA in DHi (-8%; **Fig. 4**) and a

decrease of PE in VHi (-14%; data not shown). No impact of Mn^{2+} in IHi and in the contralateral hippocampus could be detected (DHc, IHc and VHc; data not shown).

In **Figure 5**, we can observe that metabolite amplitudes are unaffected by Mn^{2+} in all 3 parts of hippocampus (DH, IH and VH) in both ipsi- and contra-hippocampus, except for PE (-14%) in the VHi. All metabolites except PE are normal in the VH (Fig. 4 and data not shown). Finally, we observed a linear correlation of the metabolite amplitude of Glu, PE and GABA, with Mn^{2+} concentration estimated by MRI (**sup Fig.1**).

INSERT FIG. 4

INSERT FIG. 5

DISCUSSION

In this study, we characterized the impact of a high (500 nmol) and low (8 nmol) dose of Mn^{2+} on the hippocampal metabolism by ^{1}H HRMAS MRS, in different sub-regions of the hippocampus. The ^{1}H HRMAS MRS technique was particularly well suited for this aim because it provided highly resolved spectra from 15 µl hippocampal samples. At 500 nmol, Mn^{2+} injection resulted in two main effects: (i) one linked to paramagnetic properties of Mn^{2+}, i.e. a T_1 reduction and a line broadening of specific resonances, (ii) a strong biological effect on hippocampal metabolism. No significant effects were detected at 8 nmol of $MnCl_2$.

Metabolism

NAA, produced by mitochondria, is generally used as a marker of neuronal death or severe neuronal dysfunction [26]. In many diseases and brain injuries (epilepsy, amyotrophic lateral sclerosis ischemia, stroke and trauma), a decrease of NAA between 15 and 80% has been reported [26]. In our study, high-dose (500 nmol) Mn^{2+} injection induced a 19% decrease in NAA amplitude at the injection site, and a 13% decrease both in the IHi and in the controlateral equivalent (DHc). However in the latter area, we did not observe any neuronal death by using specific NeuN labeling [22], indicating that the decrease in NAA could be a consequence of neuronal or mitochondrial dysfunction [15]. Similarly, Zwingmann et al. observed a decrease in NAA (-28%) in the rat globus pallidus; however, they administered Mn^{2+} intra-peritoneally at a dose of 50 mg/Kg during 4 consecutive days ([13] to reproduce the human chronic intoxication). For the lowest Mn^{2+} dose (8 nmol), the NAA decrease was limited to 8% of the control value and was restricted to the injection site. This limited impact on hippocampal metabolism is in agreement with literature showing no effects on synaptic plasticity and memory performance after injection of a low dose of

Mn^{2+} (subcutaneous injection of 0.1 mmol/Kg or intraperitoneal injection of 0.2 mmol/Kg) [27,28]. In addition to a NAA lowering, the high Mn^{2+} dose led to an increase of Ala and Glu and a decrease of GABA, whereas Gln amplitude did not change. These results are in agreement with what has been observed in the frontal cortex by NMR spectroscopy following 4-day Mn^{2+} treatment (50 mg/kg/day) [13]. The amount of m-Ins, an organic osmolyte implicated in the regulation of astrocyte's volume [29], decreased at the injection site. This suggests a local astroglyosis, which is in line with previous histological reports following local Mn^{2+} injection [22,30]. For both injection quantities, the impact on metabolism appears to be correlated to the Mn^{2+} concentration along hippocampus (**Fig.1 Supp**). We previously showed that a Mn^{2+} injection in the DG of the hippocampus (500 nmol) led to a Mn concentration of 0.458 mM in the DHc [22]. Using the linear regression described in **Fig.2 Supp**, we estimated the metabolite amplitudes corresponding to this Mn^{2+} concentration (0.458 mM). We found amplitude values of 0.04, 0.006, .009 and 0.002, very close to the experimental values (0.06, 0.004, 0.008 and 0.002 for Glu, PE, GABA and PC respectively) in the DHc. These results suggest that local Mn^{2+} concentration could be a predictor of Mn^{2+} impact on metabolism. This local Mn^{2+} concentration can be determined using T_1 map in MRI. Conversely, the metabolite amplitude could be a predictor of Mn^{2+} concentration. However a dose study is required to properly demonstrate the correlation between metabolite amplitude and Mn^{2+} concentration. The impact of the high dose of Mn^{2+} on metabolites was important also in the contralateral hippocampus. T_1-weighted images, 24h after injection of Mn^{2+}, show a diffusion of Mn in the brain, compared to the low dose. A higher volume has been used for the high dose (10 µL instead of 80 nL for the low dose) that could induce diffusion of Mn^{2+} via the blood stream and ventricles. This diffusion might explain the high impact

of Mn^{2+} in the contralateral hippocampus. However, no significant difference in metabolite amplitude was observed between controls (injection of 10 µL or 80 nL of vehicle solution), indicating a poor impact of the injection volume. So the impact of Mn on hippocampal metabolism is more likely due to Mn dose than to Mn injected volume. In follow-up studies, the impact of repeated Mn injections may however differ from that of a single injection.

Mn^{2+} chelation

After Mn^{2+} injection, we observed a specific broadening of Lac, Glu, NAA and Asp resonances, whereas other peaks remained unaffected. This broadening (not observed after injection of vehicle) is due to Mn^{2+} paramagnetic effect, indicating that Mn^{2+} is still present in the tissue 24h after its injection and that it is in close vicinity to the proton groups whose resonances are broadened. It has previously been reported that Mn^{2+} could be chelated by the organic acids [31]. Further studies should evaluate the stoichiometry and the apparent affinity constant of the formed complexes [32] by using other analytical methods like conductimetry or relaxometry. Indeed, MRS observables like chemical shifts or T_1 are strongly affected by the important paramagnetic effect of Mn^{2+}, which preclude the use of such methods. According to the differential broadening observed *in vitro* on the Glu resonances (data not shown), we could postulate that Mn^{2+} is chelated by the carboxylic acid when no amine group is present in its close vicinity. This could explain why Gln resonances, with two amine groups close to acid groups, are not broadened.

Mn relaxivity and concentration

The experiment performed *in vitro* to assess the competition between m-Ins and Lac for Mn^{2+} chelation demonstrated that, like *in vivo*, Mn^{2+} was specifically chelated by Lac. This chelation, which impacts the Mn^{2+} relaxivity, suggests that Mn^{2+}

concentrations assessed by T_1 measurements *in vivo* could be overestimated. However, there is a good data consistency between MEMRI and ^{1}H HRMAS MRS. It is therefore possible that the T_1 lowering of water in presence of Lac observed *ex vivo* is not detectable *in vivo*, due to the lower sensibility of *in vivo* MRI.

Conclusion

MEMRI is a useful tool to study tract-tracing and Mn^{2+} transport. Usual Mn^{2+} concentrations used in MEMRI are between 50 and 100 mM with an injection volume below 1 µL. This corresponds to the low Mn^{2+} dose used in this study. This dose (around 8 nmol) has only a small impact on the hippocampus metabolism. On the other hand, a high Mn^{2+} dose (500 nmol), resulted in two main effects: first, an effect linked to paramagnetic properties of Mn^{2+}; second, a biological effect on brain metabolism and function. This high Mn^{2+} dose does not seem appropriate for MEMRI experiment. Finally, our result reveals an interesting property of Mn^{2+} on organic acid resonance broadening, suggesting a specific chelation of Mn^{2+}. This chelation directly impacts Mn^{2+} relaxivity, suggesting an overestimation of Mn^{2+} concentration when assessed using T_1.

EXPERIMENTAL

Animals and protocol

A total of 36 female, 3-month-old, Sprague–Dawley rats (230±11 g, Charles Rivers, France) were used. All experiments were approved by the local ethic committee and were in full compliance with the guidelines of the European community (EUVD 86/609/ EEC) for the care and use of the laboratory animals. Efforts were made to limit the number of animals used. All procedures were performed under isoflurane (IsoFlo, Axience, France) anesthesia (5% for induction, maintenance under 2.5%).

Rectal temperature was monitored and maintained at 37°C with a heating pad. Two experiments with different manganese quantities were used on this protocol:

- Experiment 1 (high dose) - 50 mM hydrated manganese chloride ($MnCl_2$–$4H_2O$, M1787, Sigma-Aldrich, St Louis, MO, USA) were dissolved in 400 mM bicine saline and pH was adjusted to 7.3 by adding NaOH to reach a physiological value of osmolarity (300 mOsm/L). Rats received an intracerebral (IC) injection of 10 µL of either $MnCl_2$ 50 mM (500 nmol) (n=8) or of vehicle solution (n=8; control animals).
- Experiment 2 (low dose) – 100 mM hydrated manganese chloride were dissolved in distilled water and 10 mM Tris-HCl to a final pH of 7.3 and osmolarity of 300 mOsm/L. Rats received an IC injection of either 80 nL of $MnCl_2$ 100 mM (8 nmol) (n=10) or of vehicle solution (n=10; control animals).

For both experiments, the $MnCl_2$ solution was filtered through 0.2-µm membranes prior to injection.

Surgery and tracer injection

$MnCl_2$ was injected in the dentate gyrus of the right dorsal hippocampus, as previously described [22] (**Fig. 6A**). Briefly, animals were placed in a stereotaxic frame and xylocain (Vétoquinol, France) was applied prior to the scalp incision. Bregma, the sagittal suture, and the surface of the brain were used as references for anterior-posterior (−3.24 mm), lateral (−1.2 mm) and ventral (−4.0 mm) coordinates, respectively [33]. For the experiment 1, 10 µL of $MnCl_2$ solution at 50 mM was instilled at a rate of 0.5 µL/min with a 32-gauge Hamilton syringe needle. For the experiment 2, 80 nL of $MnCl_2$ solution at 100 mM was instilled at a rate of 8 nL/min with a 34 G silice cannula (Phymep, France). The syringe or cannula was left in place 10 minutes

and was retracted stepwise to prevent tracer leakage along the needle track. The wound was disinfected with Vetadine (Vétoquinol, France) and sutured.

In the following, the injected hemisphere is called ipsilateral and the other, contralateral.

***In vivo* MRI experiments**

MRI was performed 24 h after $MnCl_2$ injection. The animals were placed in a dedicated cradle equipped with byte and ear bars. Temperature and breath rate were monitored during the acquisition. The experiments were carried out in a horizontal 7 T MRI system (Avance III, Bruker, Ettlingen, Germany) using a surface/volume cross coil configuration. T_1-weighted images were obtained using a TurboRare 3D sequence, TR=300 ms, Effective TE=12 ms, matrix 128×128×64, FOV=16×16×32 mm, voxel size=0.125×0.125×0.5 mm and echo-train length=6. The acquisition duration was 14 min. A T_1 map, with a lower spatial resolution, was obtained using a saturation recovery approach (Spin-Echo, 18 TR, in the range of [30–3750] ms, TE=7.8 ms, matrix 128×128, FOV=28×28 mm, slice thickness=1 mm, 1 slice, and voxel size=0.22×0.22 mm). The acquisition duration was 17 min.

MRI data were analyzed using software developed in the Matlab environment (Mathworks, Natick, MA, USA). T_1 maps were derived by fitting a two-parameter monoexponential recovery function to the saturation-recovery data, using a non-linear fitting algorithm. T_1 values were eventually converted to Mn^{2+} concentrations using the following formula where T_1 is the longitudinal relaxation time of the sample (second), T_1w is the longitudinal relaxation time of water (2.85 seconds), r1 is the Mn^{2+} relaxivity at 7T (6.7 mM^{-1} s^{-1} [34]) and $[Mn^{2+}]$ is the Mn^{2+} concentration in the tissue (mM).

$$\frac{1}{T1} = \frac{1}{T1w} + r1 \,.\, [Mn^{2+}]$$

Seven regions of interest (ROI) were manually drawn: the background noise, the dorsal, the intermediary and the ventral hippocampus (DH, IH and VH, respectively) in each contralateral and ipsilateral hippocampus.

INSERT FIG. 6

***Ex vivo* ^{1}H HRMAS MRS of biopsies**

Sample preparation

24 h after $MnCl_2$ injection and immediately after MRI, anesthetized rats were decapitated and the brain rapidly removed; the whole hippocampus was rapidly dissected on ice at 4°C, and each ipsilateral (i) and contralateral (c) part was divided in three pieces of equal size named dorsal (DH), intermediate (IH) and ventral hippocampus (VH), corresponding to the ROI analyzed by MRI. Six biopsies per animal (**Fig. 6B**) DHi, IHi, VHi, DHc, IHc and VHc were then sampled and immediately frozen in liquid nitrogen. Approximately 15 mg of the frozen biopsy were rapidly introduced in a 4 mm ZrO_2 rotor and 30 µL of a cold 1 mM D_2O solution of 3-(trimetylsilyl) propionic-2,2,3,3-d_4 acid (TSP) was added as chemical shift internal standard (δ=0 ppm) (EURISOTOP, France). The rotor was fitted with a 50-µL spherical insert and transferred in the NMR probe, which had been previously cooled at 4°C. The entire HRMAS study was performed at this temperature. The acquisition started after 10 min of sample rotation to reach temperature equilibrium.

HRMAS data acquisition

Spectra were recorded on a Bruker Avance 400 spectrometer (proton frequency 400.13 MHz), equipped with a 4 mm ^{1}H-^{13}C-^{31}P HRMAS probe-head. Samples were spun at 4000 Hz. 1D spectra were all acquired with a Carr-Purcell-Meiboom-Gill (CPMG) pulse sequence to attenuate macromolecule and lipid resonances, synchronized with the spinning rate (interpulse delay: 250 µs, total spin echo time: 30

ms). Residual water signal was presaturated during the 2 s relaxation delay time. Total acquisition of one spectrum with 256 scans lasted 16 min. Resonance assignment was performed as previously described [35].

HRMAS data processing

For quantification, the QUEST procedure of the jMRUI algorithm was used with a simulated database including the following metabolites: acetate (Ace), alanine (Ala), aspartate (Asp), creatine and phosphocreatine (Cr), choline (Cho), γ-amino-butyric acid (GABA), glutamate (Glu), glutamine (Gln), glutathione (Gsh), glycerophosphocholine (GPC), glycine (Gly), lactate (Lac), myo-inositol (m-Ins), N-acetylaspartate (NAA), phosphoethanolamine (PE), phosphocholine (PC), scyllo-inositol (s-Ins) and taurine (Tau). The first 16 data points were used to model the background signal of macromolecules and lipids, which were not totally removed by the 30 ms CPMG. The amplitude of metabolites calculated by QUEST was normalized to the total spectrum signal and then only relative concentrations were produced. Using this method, 18 metabolites could be quantified directly from our brain biopsies [24,35]. In some spectra, Asp, Glu, Lac and NAA experienced line broadening due to Mn^{2+} paramagnetic effect. The quantification became unreliable, even when allowing an extra-damping constraint to 10 Hz in the QUEST procedure. To account for this broadening, two metabolite databases were used: one classical for all metabolites, with 2 Hz linewidth and one with broader resonances (≅10 Hz) for Asp, Glu, Lac and NAA. The Cramer Rao lower bounds (CRLB) determined by the jMRUI algorithm estimate the standard deviation of the fit for each metabolite. For most of the metabolites and for all quantifications, we obtained CRBL ≤5%, and CRBL ≤25% for Ace, Asp, s-Ins and Gsh. All metabolites were therefore used for statistics.

In vitro ^{1}H HRMAS MRS of Mn^{2+} solutions

Calibrations curves

$MnCl_2$, m-Ins ($C_6H_{12}O_6$) and Lac ($CH_3CH(OH)COOLi$) (Sigma Aldrich, La Verpillère, France) were dissolved in the same TSP/D_2O solution as that used for biopsies (see above). Samples with variable concentrations of $MnCl_2$ (0 to 100 µM) and fixed concentrations of Lac (8 mM) and m-Ins (8 mM) were prepared. Rotors (50-µL) were fitted with 30 µL of the total solution, and measurements were obtained with the same acquisition parameters used for the biopsy experiments, i.e. 4 KHz spinning rate and a 30-ms CPMG sequence. A lorentzian filtering of 0.3 Hz was applied to all signals before Fourier transform. An automatic baseline correction was applied and chemical shifts aligned relative to TSP at 0 ppm. For linewidth measurement, the width at half height of a given peak was measured with the Bruker software Topspin 3.0; the whole massif was considered, including scalar coupling constants.

Using this method, the linewidth of Lac CH_3 (1.33 ppm) and m-Ins CH (3.62 ppm) peaks were plotted versus Mn^{2+} concentrations (**Fig. 3**).

T_1 measurements

T_1 of H_2O protons (residual peak of 99.9% D_2O) and of Lac (8 mM in 99.9% D_2O) were measured with and without 20 µM of $MnCl_2$, a concentration sufficient to broaden Lac. These concentrations of both Lac and Mn^{2+} were also chosen because they were approximately equivalent to the concentrations in our biopsies. An inversion-recovery sequence and the Topspin 3.0 procedure were used to measure T_1 without water suppression. T_1 values recapitulated in table1 are mean values of two replicates.

Statistical analysis

All results are expressed as mean ± standard error of the mean (SEM). All the comparisons presented were parametric unpaired t-tests performed using Excel software. To evaluate whether the broadening is a predictor of the Mn^{2+} concentration, the Pearson correlation coefficient was computed.

A p value < 0.05 was considered significant.

ACKNOWLEDGEMENTS

The authors acknowledge the support of the MRI Facility of Grenoble (IRMaGe). AD received a stipend from the Région Rhône-Alpes – Cluster HVN.

REFERENCES

1. M. Aschner, B. Lukey and A. Tremblay, *Neurotoxicology*, 2006, **27**, 733–736.
2. M. S. Golub, C. E. Hogrefe, S. L. Germann, T. T. Tran, J. L. Beard, F. M. Crinella and B. Lonnerdal, *Neurotoxicol Teratol*, 2005, **27**, 615–627.
3. A. P. Koretsky and A. C. Silva, *NMR Biomed*, 2004, **17**, 527–531.
4. K. Narita, F. Kawasaki and H. Kita, *Brain Res*, 1990, **510**, 289–295.
5. R. G. Pautler, *NMR Biomed*, 2004, **17**, 595–601.
6. A. Daoust, S. Bohic, Y. Saoudi, C. Debacker, S. Gory-Fauré, A. Andrieux, E. L. Barbier and J.-C. Deloulme, *Neuroimage*, 2014, **96**, 133–142.
7. D. J. Jung, M. Han, S.-U. Jin, S. H. Lee, I. Park, H.-J. Cho, T.-J. Kwon, H. J. Lee, J. H. Cho, K.-Y. Lee and Y. Chang, *Neuroimage*, 2014, **100**, 642–649.
8. T.-H. Lin, J. H. Kim, C. Perez-Torres, C.-W. Chiang, K. Trinkaus, A. H. Cross and S.-K. Song, *Neuroimage*, 2014, **100**, 244–253.
9. X. Yu, S. Chung, D.-Y. Chen, S. Wang, S. J. Dodd, J. R. Walters, J. T. R. Isaac and A. P. Koretsky, *Neuron*, 2012, **74**, 731–742.
10. T. Majid, Y. O. Ali, D. V. Venkitaramani, M.-K. Jang, H.-C. Lu and R. G. Pautler, *Neuroimage Clin*, 2014, **4**, 711–717.
11. Y. Chang, S.-T. Woo, J.-J. Lee, H.-J. Song, H. J. Lee, D.-S. Yoo, S. H. Kim, H. Lee, Y. J. Kwon, H. J. Ahn, J.-H. Ahn, S.-J. Park, Y. C. Weon, I.-S. Chung, K. S. Jeong and Y. Kim, *NeuroToxicology*, 2009, **30**, 950–957.
12. C. Zwingmann, D. Leibfritz and A. S. Hazell, *Neurotoxicology*, 2004, **25**, 573–587.
13. C. Zwingmann, D. Leibfritz and A. S. Hazell, *Glia*, 2007, **55**, 1610–1617.
14. C. Zwingmann, D. Leibfritz and A. S. Hazell, *J. Cereb. Blood Flow Metab.*, 2003, **23**, 756–771.

15. A. Daoust, Y. Saoudi, J. Brocard, N. Collomb, C. Batandier, M. Bisbal, M. Salomé, A. Andrieux, S. Bohic and E. L. Barbier, *Hippocampus*, 2014, **24**, 598–610.
16. E. A. Malecki, *Brain Research Bulletin*, 2001, **55**, 225–228.
17. G. V. Malthankar, B. K. White, A. Bhushan, C. K. Daniels, K. J. Rodnick and J. C. K. Lai, *Neurochemical Research*, 2004, **29**, 709–717.
18. I. Aoki, Y.-J. L. Wu, A. C. Silva, R. M. Lynch and A. P. Koretsky, *Neuroimage*, 2004, **22**, 1046–1059.
19. Smith, V. Kallhoff, H. Zheng and R. G. Pautler, *Neuroimage*, 2007, **35**, 1401–1408.
20. S. Canals, M. Beyerlein, A. L. Keller, Y. Murayama and N. K. Logothetis, *NeuroImage*, 2008, **40**, 458–472.
21. W. N. Sloot, A. J. van der Sluijs-Gelling and J. B. P. Grambbergen, *Journal of Neurochemistry*, 1994, **62**, 205–216.
22. A. Daoust, E. L. Barbier and S. Bohic, *NeuroImage*, 2013, **64**, 10–18.
23. A. Van der Linden, M. Verhoye, V. Van Meir, I. Tindemans, M. Eens, P. Absil and J. Balthazart, *Neuroscience*, 2002, **112**, 467–474.
24. H. Rabeson, F. Fauvelle, G. Testylier, A. Foquin, P. Carpentier, F. Dorandeu, D. van Ormondt and D. Graveron-Demilly, *Magnetic Resonance in Medicine*, 2008, **59**, 1266–1273.
25. O. Beckonert, M. Coen, H. C. Keun, Y. Wang, T. M. D. Ebbels, E. Holmes, J. C. Lindon and J. K. Nicholson, *Nat Protoc*, 2010, **5**, 1019–1032.
26. J. R. Moffett, B. Ross, P. Arun, C. N. Madhavarao and M. A. A. Namboodiri, *Prog Neurobiol*, 2007, **81**, 89–131.
27. O. Eschenko, S. Canals, I. Simanova and N. K. Logothetis, *Magnetic Resonance Imaging*, 2010, **28**, 1165–1174.

28. S. J. Jackson, R. Hussey, M. A. Jansen, G. D. Merrifield, I. Marshall, A. MacLullich, J. L. W. Yau and T. Bast, *Behavioural Brain Research*, 2011, **216**, 293–300.
29. J. F. Le Bas, F. Estève, S. Grand, C. Rubin, C. Rémy, A. L. Benabid and M. Décorps, *J Neuroradiol*, 1998, **25**, 55–69.
30. A. S. Hazell, L. Normandin, B. Nguyen and G. Kennedy, *Neuroscience Letters*, 2003, **349**, 13–16.
31. K. Kishi, H. Wariishi, L. Marquez, H. B. Dunford and M. H. Gold, *Biochemistry*, 1994, **33**, 8694–8701.
32. P. Job, *Compt. Rend. Acad. Sci.*, 1925, **180**, 928–930.
33. G. Paxinos and C. Watson, *The Rat Brain in Stereotaxic Coordinates - The New Coronal Set, Fifth Edition*, Academic Press, 5th edn., 2004.
34. A. C. Silva, J. H. Lee, I. Aoki and A. P. Koretsky, *NMR Biomed*, 2004, **17**, 532–543.
35. F. Fauvelle, F. Dorandeu, P. Carpentier, A. Foquin, H. Rabeson, D. Graveron-Demilly, P. Arvers and G. Testylier, *Toxicology*, 2010, **267**, 99–111.

FIGURE CAPTIONS

Fig. 1: *In vivo* MRI images and Mn^{2+} concentration derived from T_1 map in the hippocampus after injection of two different Mn^{2+} doses.

A. T_1-weighted images 24 h after intra-hippocampal Mn^{2+} injection. Images correspond to a coronal section, showing the dorsal hippocampus. At a high dose (500 nmol), Mn^{2+} is distributed throughout the brain with a high intensity in both hippocampi. At a low dose (8 nmol), Mn^{2+} accumulates mainly in ipsilateral DG and CA3 of the hippocampus (see Fig. 6 for anatomical reference).

B. Concentration of Mn^{2+} derived from T_1 values (Mn relaxivity r1= 6.7 $mMol^{-1}$ s^{-1}) in dorsal, intermediary and ventral hippocampus (DH, IH and VH, respectively) and in ipsi and contralateral hemispheres. In both injections, Mn^{2+} concentration decreases along hippocampus from DH (injection site) to VH.

C. Table of Mn^{2+} concentrations derived from T_1 map in the 6 hippocampus sub-regions after injection of Mn^{2+} (low and high doses). Controls received the vehicle injection corresponding to low and high doses.

High dose: n=8 controls; n=8 Mn^{2+} injected rats; p is the comparison of T_1 value between 500 nmol $MnCl_2$ and control high dose animals ** $p<0.005$; *** $p<0.0001$. Low dose: n=10 control; n=10 Mn^{2+} injected rats. p is the comparison of T_1 value between 8 nmol $MnCl_2$ and control low dose animals ** $p<0.005$; *** $p<0.0001$. Mean ± SEM.

Fig. 2: *Ex vivo* ^{1}H HRMAS MRS spectra after Mn^{2+} injection (500 nmol) in the injected hippocampus site.

Representative spectra obtained from a hippocampal biopsy of a Mn^{2+} injected (bottom) and a control (top) rat. In the dorsal ipsilateral hippocampus (DHi, injection site), some resonances were broadened due to the Mn paramagnetic effect (see arrows), mainly lactate (Lac), N-acetylaspartate (NAA), glutamate (Glu) and aspartate (Asp) resonances, whereas for exemple taurine (Tau) or alanine (Ala) were not affected. No broadening was observed in intermediary and ventral ipsilateral hippocampus (IHi and VHi).

Fig. 3: I*n vitro* Mn^{2+} broadening effect on ^{1}H HRMAS MRS spectra of solutions

Linewidth of lactate (Lac) CH_3 (1.33 ppm) and myo-inositol (m-Ins) CH (3.62 ppm) resonances as a function of Mn^{2+} concentration (n=9). The solutions contained 8 mM of Lac, 8 mM of m-Ins and various concentrations of Mn (0-100 µM).

The linewidth of Lac CH_3 resonance is proportional to Mn^{2+} concentration ($p<0.00001$) but not that of m-Ins ($p=0.4$).

Figure 4: Metabolite amplitude in the injected hippocampus measured *ex vivo* by ^{1}H HRMAS MRS.

Metabolite amplitude after an injection of a high (500 nmol) and low (8 nmol) Mn^{2+} doses in the ipsilateral dorsal hippocampus (DHi), quantified using jMRUI software. A significant impact is observed after a high-dose Mn^{2+} injection compared to the low dose.

High dose: n=8 controls; n=8 Mn^{2+} injected rats. Low dose: n=10 control; n=10 Mn^{2+} injected rats. *p<0.05, **p<0.01, ***p<0.001 (mean ± SEM).

Abbreviations: Ala: alanine; Asp: aspartate; Cho: choline; GABA: γ-aminobutyric acid; Glu: glutamate; m-Ins: myo-inositol; NAA: N-acetyl aspartate; Lac: lactate; PC: phosphorylcholine; PCr: phosphocreatine; PE: phosphoethanolamine.

Figure 5: Evolution of metabolite amplitudes along hippocampus after Mn^{2+} injection

Amplitude average of the metabolite signal obtained by *ex vivo* ^1H HRMAS MRS. It is expressed as a fraction of the corresponding control sample along the 3 parts of the hippocampus: dorsal, intermediary and ventral hippocampus (DH, IH and VH, respectively), in ipsi (i) and contralateral (c) hemispheres. After a high Mn^{2+} injection (500 nmol), the amplitudes of glutamate, γ-aminobutyric acid, phosphorylcholine and phosphoethanolamine (Glu, GABA, PC and PE, respectively), decrease along the hippocampus (**A**). After a lower Mn^{2+} dose (8 nmol), there is no significant perturbation for all metabolites except for PE in the VHi (**B**).

High dose: n=8 controls; n=8 Mn^{2+} injected rats. Low dose: n=10 control; n=10 Mn^{2+} injected rats. *p<0.05, **p<0.01, ***p<0.001 (mean ± SEM).

Fig. 6: intra-cerebral injection of Mn^{2+} and location of hippocampal sub-regions biopsies.

A. Mn^{2+} was injected in the right dentate gyrus (DG) of the rat hippocampus. The cannula or syringe used for Mn^{2+} injection is represented by a gray vertical bar. Two differents doses were used: 80 nL, 100mM (8 nmol) or 10µL, 50mM (500 nmol).

B. 24h after Mn^{2+} injection, the whole hippocampus was dissected and each ipsilateral (i) and contralateral (c) part was divided in three pieces of equally size named dorsal (DH, blue), intermediate (IH, yellow) and ventral hippocampus (VH, purple), leading to six samples for each animal. These biopsies were then used for metabolism study by ^{1}H HRMAS MRS.

Impact of manganese on the hippocampus metabolism in the context of MEMRI: a Proton HRMAS MRS study

A. Daoust, E. L. Barbier, S. Bohic, V. Stupar, S. Maunoir-Regimbal and F. Fauvelle

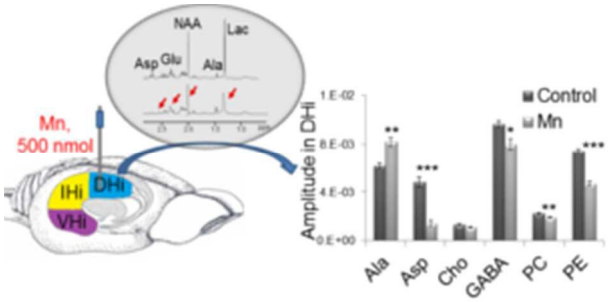

HRMAS spectrum revealed an important impact of Mn 500 nmol on hippocampal metabolism, not observed with Mn 8 nmol.

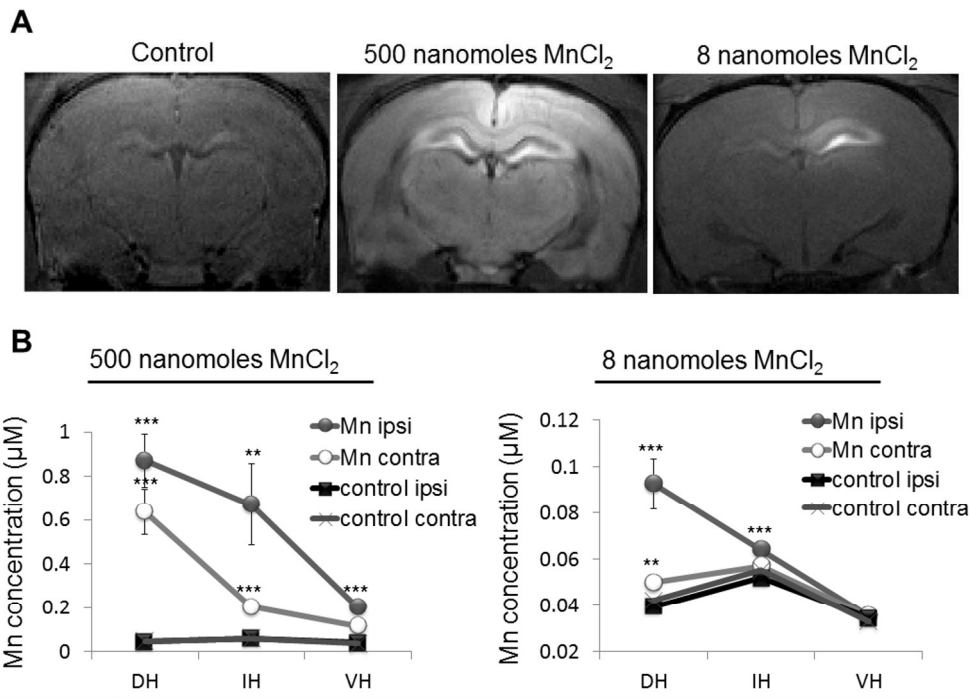

C	Mn concentration derived from T_1 map (µM)			
	Control low dose	8 nmol $MnCl_2$	Control high dose	500 nmol $MnCl_2$
DHi	40 ± 2	93 ± 11***	44 ± 6	870 ± 50***
IHi	52 ± 4	64 ± 2***	59 ± 6	670 ± 76**
VHi	35 ± 2	35 ± 2	40 ± 7	201±26***
DHc	42 ± 2	50 ± 2**	47 ± 5	636 ± 103***
IHc	55 ± 5	57 ± 1	59 ± 4	203 ± 16***
VHc	33 ± 2	35 ± 1	36 ± 2	115 ± 3***

Fig. 1: In vivo MRI images and Mn2+ concentration derived from T1 map in the hippocampus after injection of two different Mn2+ doses.

A. T1-weighted images 24 h after intra-hippocampal Mn2+ injection. Images correspond to a coronal section, showing the dorsal hippocampus. At a high dose (500 nmol), Mn2+ is distributed throughout the brain with a high intensity in both hippocampi. At a low dose (8 nmol), Mn2+ accumulates mainly in ipsilateral DG and CA3 of the hippocampus (see Fig. 6 for anatomical reference).

B. Concentration of Mn2+ derived from T1 values (Mn relaxivity r1= 6.7 mMol−1 s−1) in dorsal, intermediary and ventral hippocampus (DH, IH and VH, respectively) and in ipsi and contralateral hemispheres. In both injections, Mn2+ concentration decreases along hippocampus from DH (injection site) to VH.

C. Table of Mn2+ concentrations derived from T1 map in the 6 hippocampus sub-regions after injection of Mn2+ (low and high doses). Controls received the vehicle injection corresponding to low and high doses. High dose: n=8 controls; n=8 Mn2+ injected rats; p is the comparison of T1 value between 500 nmol MnCl2

and control high dose animals ** p<0.005; *** p<0.0001. Low dose: n=10 control; n=10 Mn2+ injected rats. p is the comparison of T1 value between 8 nmol MnCl2 and control low dose animals ** p<0.005; *** p<0.0001. Mean ± SEM.

182x222mm (600 x 600 DPI)

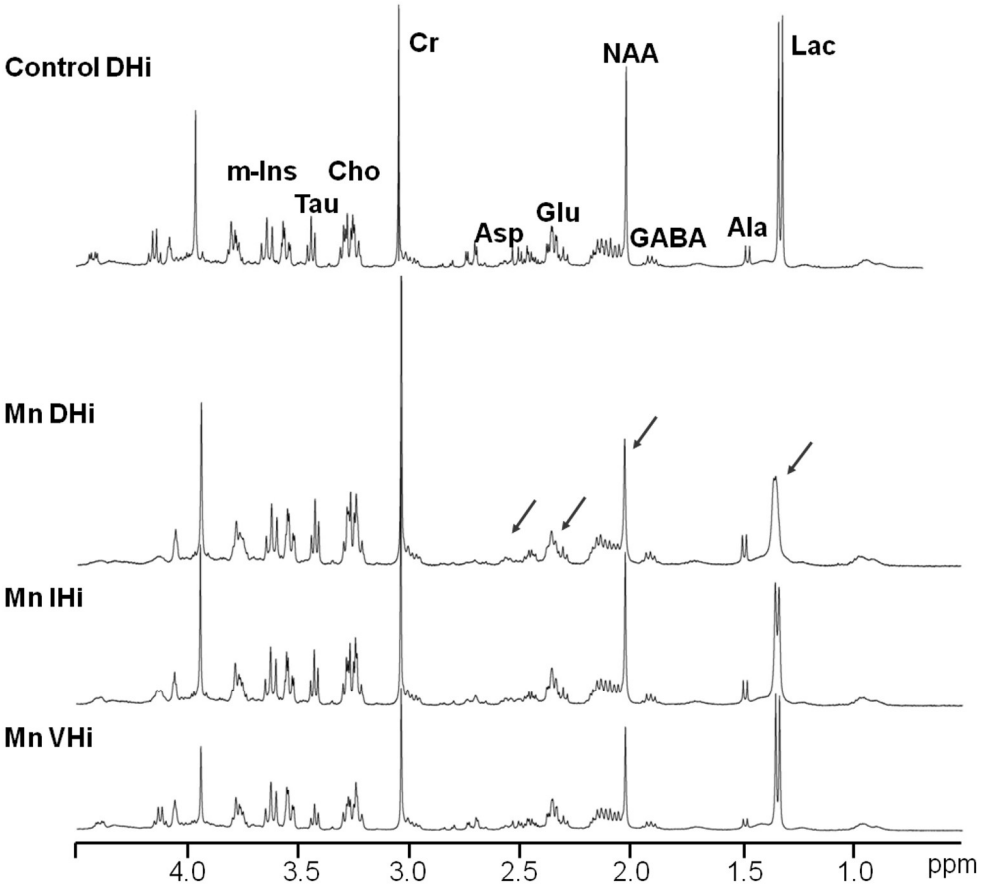

Fig. 2: Ex vivo 1H HRMAS MRS spectra after Mn2+ injection (500 nmol) in the injected hippocampus site. Representative spectra obtained from a hippocampal biopsy of a Mn2+ injected (bottom) and a control (top) rat. In the dorsal ipsilateral hippocampus (DHi, injection site), some resonances were broadened due to the Mn paramagnetic effect (see arrows), mainly lactate (Lac), N-acetylaspartate (NAA), glutamate (Glu) and aspartate (Asp) resonances, whereas for exemple taurine (Tau) or alanine (Ala) were not affected. No broadening was observed in intermediary and ventral ipsilateral hippocampus (IHi and VHi).

133x119mm (600 x 600 DPI)

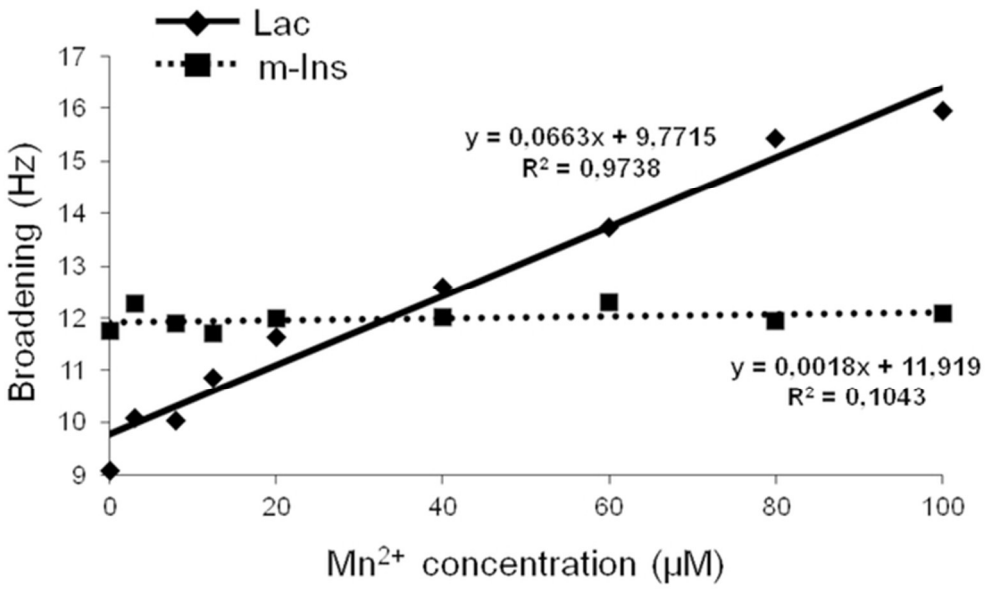

Fig. 3: In vitro Mn2+ broadening effect on 1H HRMAS MRS spectra of solutions
Linewidth of lactate (Lac) CH3 (1.33 ppm) and myo-inositol (m-Ins) CH (3.62 ppm) resonances as a function of Mn2+ concentration (n=9). The solutions contained 8 mM of Lac, 8 mM of m-Ins and various concentrations of Mn (0-100 µM).
The linewidth of Lac CH3 resonance is proportional to Mn2+ concentration ($p<0.00001$) but not that of m-Ins ($p=0.4$).

54x33mm (300 x 300 DPI)

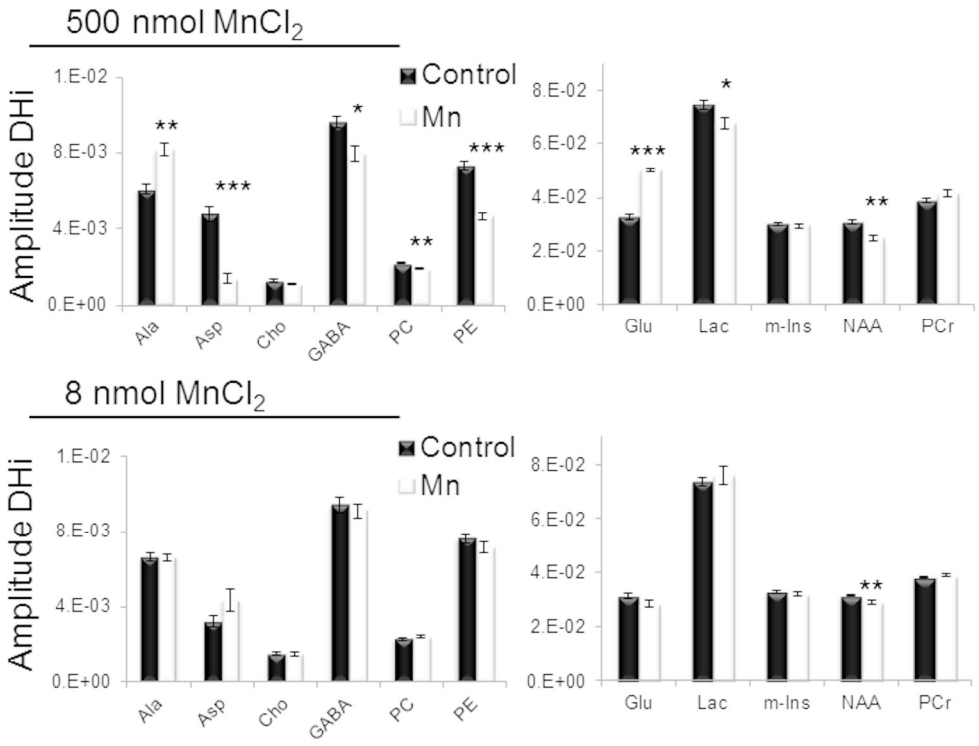

Figure 4: Metabolite amplitude in the injected hippocampus measured ex vivo by 1H HRMAS MRS. Metabolite amplitude after an injection of a high (500 nmol) and low (8 nmol) Mn2+ doses in the ipsilateral dorsal hippocampus (DHi), quantified using jMRUI software. A significant impact is observed after a high-dose Mn2+ injection compared to the low dose.
High dose: n=8 controls; n=8 Mn2+ injected rats. Low dose: n=10 control; n=10 Mn2+ injected rats. *p<0.05, **p<0.01, ***p<0.001 (mean ± SEM).
Abbreviations: Ala: alanine; Asp: aspartate; Cho: choline; GABA: γ-aminobutyric acid; Glu: glutamate; m-Ins: myo-inositol; NAA: N-acetyl aspartate; Lac: lactate; PC: phosphorylcholine; PCr: phosphocreatine; PE: phosphoethanolamine.

112x83mm (600 x 600 DPI)

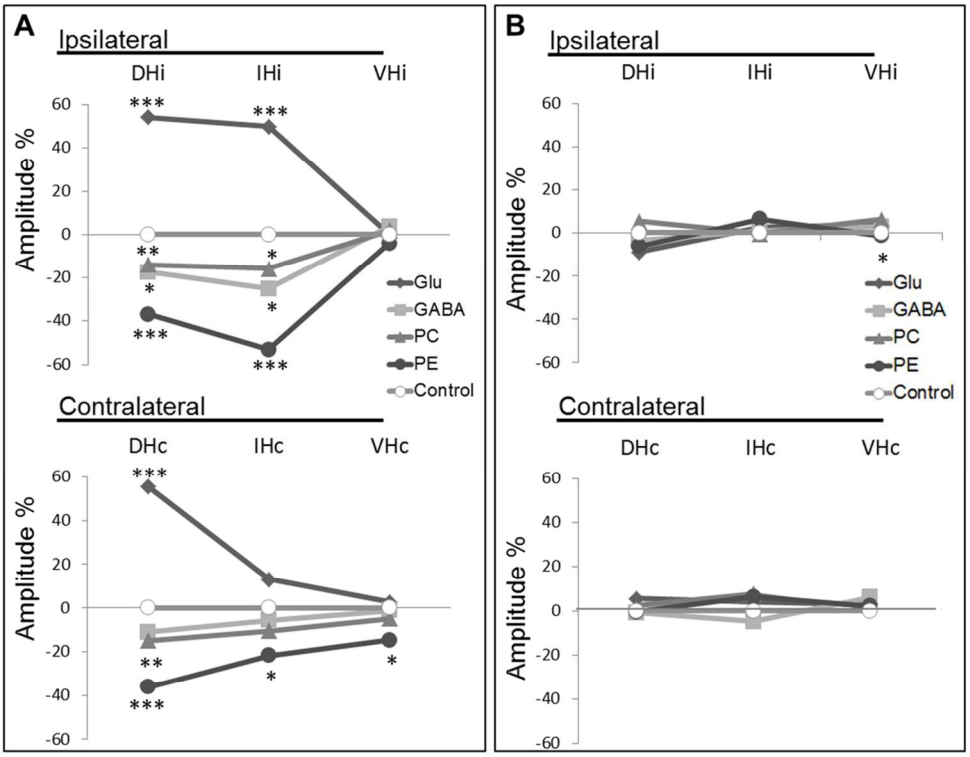

Figure 5: Evolution of metabolite amplitudes along hippocampus after Mn2+ injection
Amplitude average of the metabolite signal obtained by ex vivo 1H HRMAS MRS. It is expressed as a fraction of the corresponding control sample along the 3 parts of the hippocampus: dorsal, intermediary and ventral hippocampus (DH, IH and VH, respectively), in ipsi (i) and contralateral (c) hemispheres. After a high Mn2+ injection (500 nmol), the amplitudes of glutamate, γ-aminobutyric acid, phosphorylcholine and phosphoethanolamine (Glu, GABA, PC and PE, respectively), decrease along the hippocampus (A). After a lower Mn2+ dose (8 nmol), there is no significant perturbation for all metabolites except for PE in the VHi (B).
High dose: n=8 controls; n=8 Mn2+ injected rats. Low dose: n=10 control; n=10 Mn2+ injected rats.
*p<0.05, **p<0.01, ***p<0.001 (mean ± SEM).

49x41mm (600 x 600 DPI)

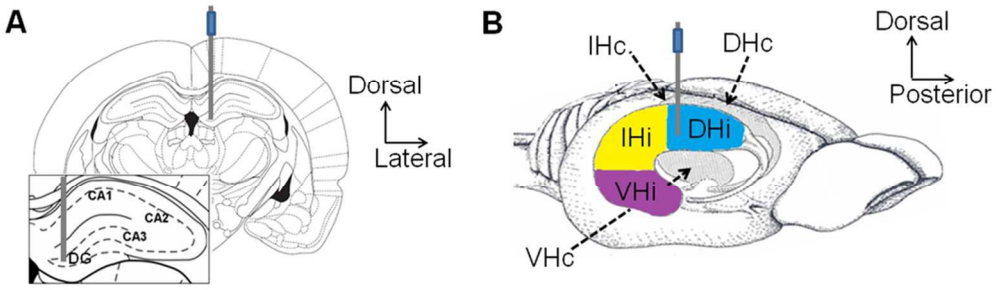

Fig. 6: intra-cerebral injection of Mn2+ and location of hippocampal sub-regions biopsies.
A. Mn2+ was injected in the right dentate gyrus (DG) of the rat hippocampus. The cannula or syringe used for Mn2+ injection is represented by a gray vertical bar. Two differents doses were used: 80 nL, 100mM (8 nmol) or 10µL, 50mM (500 nmol).
B. 24h after Mn2+ injection, the whole hippocampus was dissected and each ipsilateral (i) and contralateral (c) part was divided in three pieces of equally size named dorsal (DH, blue), intermediate (IH, yellow) and ventral hippocampus (VH, purple), leading to six samples for each animal. These biopsies were then used for metabolism study by 1H HRMAS MRS.

46x14mm (600 x 600 DPI)